Anomalous transport tuned through stochastic resetting in the rugged energy landscape of a chaotic system with roughness

Yuhui Luo,[1,2] Chunhua Zeng,[1,*] Tao Huang,[1] and Bao-Quan Ai[3]

[1]*Faculty of Civil Engineering and Mechanics/Faculty of Science, Kunming University of Science and Technology, Kunming 650500, China*

[2]*School of Physics and Information Engineering, Zhaotong University, Zhaotong 657000, China*

[3]*Guangdong Provincial Key Laboratory of Quantum Engineering and Quantum Materials, GPETR Center for Quantum Precision Measurement, SPTE, South China Normal University, Guangzhou 510006, China*

(Received 3 May 2022; accepted 15 August 2022; published 22 September 2022)

Stochastic resetting causes kinetic phase transitions, whereas its underlying physical mechanism remains to be elucidated. We here investigate the anomalous transport of a particle moving in a chaotic system with a stochastic resetting and a rough potential and focus on how the stochastic resetting, roughness, and nonequilibrium noise affect the transports of the particle. We uncover the physical mechanism for stochastic resetting resulting in the anomalous transport in a nonlinear chaotic system: The particle is reset to a new basin of attraction which may be different from the initial basin of attraction from the view of dynamics. From the view of the energy landscape, the particle is reset to a new energy state of the energy landscape which may be different from the initial energy state. This resetting can lead to a kinetic phase transition between no transport and a finite net transport or between negative mobility and positive mobility. The roughness and noise also lead to the transition. Based on the mechanism, the transport of the particle can be tuned by these parameters. For example, the combination of the stochastic resetting, roughness, and noise can enhance the transport and tune negative mobility, the enhanced stability of the system, and the resonant-like activity. We analyze these results through variances (e.g., mean-squared velocity, etc.) and correlation functions (i.e., velocity autocorrelation function, position-velocity correlation function, etc.). Our results can be extensively applied in the biology, physics, and chemistry, even social system.

DOI: 10.1103/PhysRevE.106.034208

I. INTRODUCTION

Of particular interest is stochastic resetting in various research fields. Thus it has extensively been investigated in both natural [1,2] and artificial [3,4] systems since the early 2010s. Examples of stochastic resetting include the optimal search time [3], diffusion [5], mean first passage time (MFPT) [4], fluctuating interfaces [6], work fluctuations and Jarzynski equality [7], and protein searching for specific binding sites on the DNA [8]. Another example is that the process of RNA polymerization is frequently interrupted by backtracking [9,10], where RNA cleavage should be considered as a stochastic resetting process. In statistical physics, there also exist several works about stochastic resetting. Examples include nonergodicity [11,12] and restoring ergodicity [13] for the resetting of the Brownian motion. For a equilibrium system, a stochastic resetting breaks its detailed balance and drives the system into an out-of-equilibrium state [14]. Therefore, paradoxical situations can occur in the system since the laws of thermodynamics no longer possess validity. Namely, the anomalous transport arise in such out-of-equilibrium systems.

The anomalous transports (e.g., anomalous diffusion, negative mobility, etc.) have extensively been investigated in several systems with different conditions. The noise of a chaotic system can lead to anomalous transports, such as negative mobility [15] and anomalous diffusions [16]. It is well known that the dynamical behavior of a chaotic system is sensitive to initial states [17] and system parameters [18]. It should be noted that a stochastic resetting can give rise to anomalous diffusion [19]. In brief, the anomalous phenomena have intensively been investigated in out-of-equilibrium systems. However, it is unclear whether a stochastic resetting in chaotic system leads to anomalous transport (e.g., noise-enhanced stability [20] and resonant excitation [21]) or not.

Tremendous progress has recently been made toward the stochastic resetting in several research fields. Most previous works about stochastic resetting studied that the particle is generally reset to its starting point at a specified rate. However, it is worth mentioning that the stochastic resetting by a random amplitude was investigated in a recent work [22]. From an applied perspective, this resetting provides great hope to address some challenges that numerous scientific disciplines are currently facing, such as geophysical layering [22], population dynamics [23], financial markets [24,25], and germs affected by antibiotic treatment [26]. In fact, the stochastic resetting of a particle is a process for the change of the energy in a system. Namely, the stochastic resetting of the position is the change of the potential energy in the potential energy landscape of a system, in which there exist numerous types, e.g., random potential [27,28], random walk

*zchh2009@126.com

[29], random force (noise) [30], random field [31], and so on. Notice that an earlier work [32] demonstrated that the inherent structure mapping divides up the potential energy landscape into basins of attraction surrounding the minima. Additionally, another work [33] investigated the diffusion in a potential landscape with a stochastic resetting, including stable and unstable potential energy landscapes. Numerous works were done in various system with random energy models for 40 years [34–36]. Anomalous features of diffusion were studied in a substrate potential added a random potential modeled by unbiased Gaussian distribution [37]. This random potential results from how binding energy correlations affect the diffusion along with DNA. Therefore, a random potential may be considered as a stochastic resetting by a random amplitude. On the other hand, notice that several works have studied the anomalous transport of particles moving in several systems with rough potentials [38–41]. In a word, the transports induced by stochastic resetting are extensively investigated in various systems. However, the transport of a particle, moving in an out-of-equilibrium system with the stochastic resetting of a random amplitude and roughness, remains to be elucidated. What are the dynamics in the system with the stochastic resetting, and how do the resetting and roughness affect the MFPT, diffusions, or correlation functions corresponding to these transports?

The MFPT is a key quantity in physical, chemical, and biological systems. Consequently, it has intensively been investigated in numerous research fields, such as optimization [4], the transport in a disordered media [42], diffusion-limited reactions [43], spreading of diseases [44], target search processes [45], and the escape rate of an active Brownian particle [46]. Therefore, remarkable progress has been done by a growing number of theoretical investigations in understanding MFPT and its application for 20 years [47]. Stochastic resetting is extensively investigated in MFPT [48–51], the mean recovery time of RNA cleavage [10], the first-arrival statistics of random motion [52], and continuous-time random walks under Markovian resetting [53]. These studies also demonstrated that the stochastic resetting can affect kinetics behaviors.

Moreover, diffusion is well described by the theory of Brownian motion [30]. It is frequently obtained through a mean-squared displacement (MSD), corresponding to the second-order moment of the probability distribution. Namely, the MSD corresponds to the variance of the position and is frequently used to investigate the diffusion of the particle. Besides the second-order moment, the third- and fourth-order moments of a probability distribution, corresponding to skewness and kurtosis, respectively, are extensively employed to investigate various diffusions. For example, earlier works employed the excess kurtosis and/or skewness to study the ergodicity of diffusion [30] and identified whether the angle-averaged non-Gaussian parameter is Gaussian [54]. These quantities have excellently described the types of the diffusion of the particle. Examples include the skewness for instantaneous current fluctuations in a dusty plasma experimentally [55] and the universal relation between skewness and kurtosis in complex dynamics [56]. Additionally, to our knowledge, except for MSD and the mean-squared velocity, no previous works investigate the diffusion via the mean-squared acceleration and the variance of the position-velocity, position-acceleration, or velocity-acceleration. It is unclear whether these variances characterize the types of diffusion.

Another important quantity characterizing the diffusion is the correlation function. The positive and negative values for the correlation function of the velocity indicate superdiffusion and subdiffusion, respectively. And no correlation corresponds to normal diffusion [57,58]. Most previous works studied anomalous transports or diffusions through the position autocorrelation function [59] or the velocity autocorrelation function [57]. Moreover, the space-time velocity correlation functions were used to experimentally study cold atom dynamics in an optical potential and charge transport on micro- and nanoscales [29]. The spatiotemporal velocity-velocity correlation function was employed to study a turbulence [60]. Interestingly, the position-velocity correlation was used to investigate anomalous diffusion in a recent work [61]. Additionally, the potential correlation function and density-density correlation function were employed to study probing entanglement in a many-body-localized system [62]. Furthermore, the near-neighbor spatial correlation is used to characterize critical slowing down [63]. However, to the best of our knowledge, no previous works study the correlation functions of the acceleration-acceleration, position-acceleration, and velocity-acceleration in anomalous transports. Therefore, to our knowledge, whether the kinds of diffusion are featured via these correlation functions remains poorly understood in the system.

The mentioned above raise the natural question: Can the stochastic resetting of a random amplitude lead to a kinetic phase transition or anomalous transport? If the answers are positive, what is the underlying mechanism behind these results? To address these questions, we here focus on the mechanism for the transport of the particle moving in a system with roughnesses and the stochastic resetting of a random amplitude. The system is also driven by out-of-equilibrium driving forces, i.e., an external time-periodic force, an external constant bias, and a nonequilibrium noise. Here we introduce a general numerical method that constructs the phase-space map, which guides our understanding of how a particle moves on the energy landscape of a chaotic system with the stochastic resetting and roughnesses. The method identifies the transition state between the energy barriers.

The structure of the rest paper is as follows. We first introduce a system with a rough potential and stochastic resetting of a random amplitude and present the method of our numerical simulation. We then analyze the dynamics via the bifurcation diagram, basin of attraction, and rugged energy landscape for the deterministic system and provide the physical mechanism of the transport. Then, based on the mechanism, the transport of the particle is tuned via the stochastic resetting, roughness, and noise. Furthermore, we analyze our findings through several variances (i.e., mean-squared velocity, etc.) and normalized correlation functions (NCFs) corresponding to anomalous transports. We present our conclusions at the end.

II. THE MODEL

We here consider an inertial particle moving in a system with a rough potential and stochastic resetting by a random

amplitude. It is driven by a nonequilibrium fluctuation, an external constant bias F, and an external time-dependent periodic force $A\cos(\omega t)$ with the amplitude A and the angular frequency ω. Thus the particle evolves as [38,39]

$$ma(t) + \gamma v(t) = -\frac{dU[x(t)]}{dx(t)} + A\cos(\omega t) + F + \xi(t), \quad (1)$$

where $x(t)$, $v(t)$, and $a(t)$ are the position, velocity, and acceleration of the particle at time t, respectively. m and γ denote the mass of the particle and the friction coefficient, respectively. $\xi(t)$ is a Gaussian color noise and its statistical properties are as follows:

$$\langle \xi(t) \rangle = 0, \langle \xi(t)\xi(t') \rangle = \frac{D}{\tau_0} \exp\left(-\frac{|t-t'|}{\tau_0} \right),$$

where D and τ_0 are the intensity of the noise and the correlation time, respectively. The system consists of a substrate potential $U_s(x)$ and a rough potential $U_r(x)$, namely $U(x) = U_s(x) + U_r(x)$. They are given by [40,41]

$$U_s(x) = \Delta U \sin(2\pi\omega_0 x),\ U_r(x) = -\varepsilon\cos(\omega_1 x),\ \varepsilon \ll \Delta U.$$

Here ΔU and ε is the potential barrier and the amplitude of the roughness, respectively. ω_0 and ω_1 are the frequencies of the substrate potential and the rough potential, respectively. It is required to be $\omega_0 \ll \omega_1$ to ensure that $U_r(x)$ oscillates rapidly. Therefore, here we assume $\omega_1 = 100$ and $\omega_0 = 1$. We fix $\Delta U = 1.0$ $m = 1.0$, $\gamma = 0.9$, $\tau_0 = 1.0$, $A = 4.2$, and $\omega = 4.9$, unless otherwise stated. All quantities are in dimensionless units.

The Fokker-Planck equation corresponding to the Langevin equation (1) cannot be solved in general [15,64]. Therefore, we investigate the transports and the corresponding statistical properties of the particle moving in the system through numerical simulation. We employ the fourth-order stochastic Runge-Kutta algorithm [65] with time step $\Delta t = 10^{-2}$ to discretize the Eq. (1). Then, at each step, the particle can either reset or it can evolve according to the Eq. (1). Therefore, (i) the inertial particle follows the Langevin dynamics given by Eq. (1) with probability $1 - r\Delta t$ (r is the rate of stochastic resetting) and (ii) the stochastic resetting of the particle occurs with complementary probability $r\Delta t$, namely,

$$x(t_{i+1}) = x(t_i) + \eta(t). \quad (2)$$

Here $\eta(t)$ is a random amplitude of stochastic resetting, modeled by Gaussian white noise with zero mean and unit variance. Namely, the random amplitude of stochastic resetting [22] is employed in our work.

To characterize the anomalous transports and their statistical properties, we first analyze the dynamical behaviors of the system for the deterministic dynamics through the basin of attraction, bifurcation diagram, and energy landscape. Then we focus on anomalous phenomena via the average velocity. We analyze the result through the phase-space map, NCFs, and various variances. For initial conditions, the initial positions $x(0)$ and velocities $v(0)$ are uniformly distributed over the intervals $[-1, 1]$ and $[-2, 2]$, respectively. The calculated data of the average velocity include 500 trajectories. To obtain the convergent result, 10^6 time steps of the initial transient state are removed and 10^7 time steps of the steady state are used for statistics of each trajectory. For NCFs and variances, the ensemble average contains 10^4 trajectories. Here NCFs are given by [66]

$$C_{xx}(\tau) = \frac{\langle x(t)x(t+\tau)\rangle}{\sqrt{\langle x^2(t)\rangle\langle x^2(t+\tau)\rangle}},$$
$$C_{vv}(\tau) = \frac{\langle v(t)v(t+\tau)\rangle}{\sqrt{\langle v^2(t)\rangle\langle v^2(t+\tau)\rangle}},$$
$$C_{aa}(\tau) = \frac{\langle a(t)a(t+\tau)\rangle}{\sqrt{\langle a^2(t)\rangle\langle a^2(t+\tau)\rangle}},$$
$$C_{xv}(\tau) = \frac{\langle x(t)v(t+\tau)\rangle}{\sqrt{\langle x^2(t)\rangle\langle v^2(t+\tau)\rangle}},$$
$$C_{xa}(\tau) = \frac{\langle x(t)a(t+\tau)\rangle}{\sqrt{\langle x^2(t)\rangle\langle a^2(t+\tau)\rangle}},$$
$$C_{va}(\tau) = \frac{\langle v(t)a(t+\tau)\rangle}{\sqrt{\langle v^2(t)\rangle\langle v^2(t+\tau)\rangle}}.$$

Here $C_{xx}(\tau)$, $C_{vv}(\tau)$, $C_{aa}(\tau)$, $C_{xv}(\tau)$, $C_{xa}(\tau)$, and $C_{va}(\tau)$ denote the position autocorrelation function, velocity autocorrelation function, the acceleration autocorrelation function, the position-velocity correlation function, the position-acceleration correlation function, and the velocity-acceleration correlation function, respectively. Moreover, MSD, mean-squared velocity, the mean-squared acceleration, the variances of position and velocity, position and acceleration, and velocity and acceleration are given by

$$\langle \Delta x^2(t)\rangle = \langle [x(t) - \langle x(t)\rangle]^2\rangle,$$
$$\langle \Delta v^2(t)\rangle = \langle [v(t) - \langle v(t)\rangle]^2\rangle,$$
$$\langle \Delta a^2(t)\rangle = \langle [a(t) - \langle a(t)\rangle]^2\rangle,$$
$$\langle \Delta x(t)\Delta v(t)\rangle = \langle [x(t) - \langle x(t)\rangle][v(t) - \langle v(t)\rangle]\rangle,$$
$$\langle \Delta x(t)\Delta a(t)\rangle = \langle [x(t) - \langle x(t)\rangle][a(t) - \langle a(t)\rangle]\rangle,$$
$$\langle \Delta v(t)\Delta a(t)\rangle = \langle [v(t) - \langle v(t)\rangle][a(t) - \langle a(t)\rangle]\rangle,$$

respectively.

To illustrate the anomalous transport of the particle, we analyze the findings through the energy landscape. The energy depending on the initial position x_0 and initial velocity v_0 is defined by

$$E = \frac{1}{N}\left\{ \sum_{i=1}^{N} \left(U(x_i) + \frac{1}{2}mv_i^2 \right) \right\}. \quad (3)$$

Here N is the iterations of the dynamical evolution. We here use 10^4 time steps of the steady state for each trajectory to calculate the energy. Through the energy E, we can present the energy landscape depending on the initial conditions. We also present the power for the stochastic resetting, which is defined by $P = W_{\text{reset}}/t$, where W_{reset} is given by $W_{\text{reset}} = \sum_{i=1}^{N}\{U(x_{ia}) - U(x_{ib})\}$. Here $U(x_{ia})$ and $U(x_{ib})$ indicate the potential energies after the ith stochastic resetting and before it, respectively. Namely, W_{reset} is the sum of potential energies after stochastic resettings minus those before stochastic resettings with total time t.

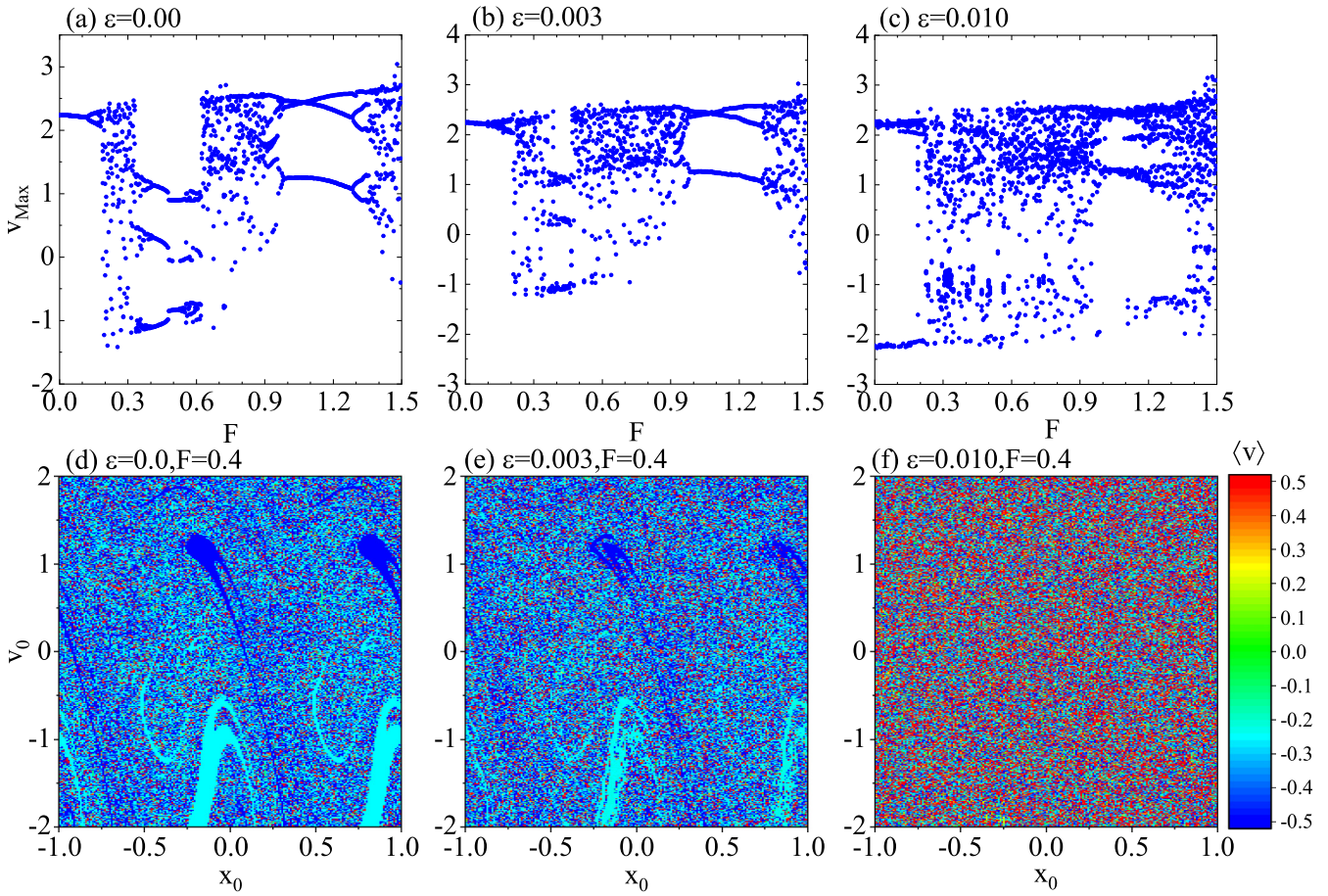

FIG. 1. The bifurcation diagram for different roughnesses $\varepsilon = 0.0$ (a), 0.003 (b), and 0.010 (c), the basins of attraction of the velocity for different roughnesses $\varepsilon = 0.0$ (d), 0.003 (e), and 0.010 (f) with $F = 0.4$ for the deterministic dynamics ($D = 0.0$).

III. THE RESULTS AND DISCUSSIONS

To understand the dynamical properties of the deterministic model ($D = 0.0$) with the roughness and without the stochastic resetting, we present the bifurcation diagram and basins of attraction in Fig. 1. The bifurcation diagram is usually used to characterize the chaotic system, suggesting that the dynamical behaviors are sensitive to the trivial variation of the system parameters. In comparison, the basin of attraction is used to characterize the dynamical properties that are sensitive to the trivial variation of initial conditions. Figure 1(a) shows that the increase of the bias F leads to the existence of period-doubling bifurcations, chaotic bands, and attractor-merging crisis for the system without the roughness. For $\varepsilon = 0.003$, Fig. 1(b) shows that the widths of chaotic bands are larger than those without the roughness. Furthermore, Fig. 1(c) shows that the chaotic bands for $\varepsilon = 0.010$ are wider than those for $\varepsilon = 0.003$. These findings suggest that chaotic behaviors occur in the system, and thus the trivial variation of the system parameters leads to the nontrivial changes of the dynamical behaviors. Additionally, we present the basin of attraction in Figs. 1(d)–1(f). Figure 1(d) shows that there exist two types of stable basins for the system without roughness. One is the cyan regime which denotes a running state $v \simeq -0.24$, and the other is the blue regime which denotes a running state $v \simeq -0.62$. This finding suggests that the dynamical behavior is sensitive to the initial condition. However, with the increase of the roughness, these basins gradually lose their stabilities, and the running states are mixed, as shown in Figs. 1(e) and 1(f). Let us now discuss the reason we get these results.

Figure 2 shows the rugged energy landscapes depending on initial position and velocity, which correspond to the basins of attraction in Figs. 1(d)–1(f). Notice that with identical system parameters, the structure of the energy landscape in Fig. 2(a) is identical to that of the basin of attraction in Fig. 1(d). Namely, $E \simeq -0.79$ and 0.92 in Fig. 2(a) correspond the basins of attraction with running states $v \simeq -0.24$ and -0.62, respectively. These results reveal that energy landscapes lead to the appearance of the basins of attraction. Namely, different energies give rise to different running states of the velocity. With the increase of the roughness, the structure of the energy landscape gradually loses its stability and becomes a mixture of states, as shown in Figs. 2(b) and 2(c). Figure 2(c) displays that for $\varepsilon = 0.01$, the rugged energy landscapes have an infinitely large population of blue spikes at low energy. Locating at these spikes, the particle cannot move, suggesting that no transport arises.

To see how the stochastic resetting affect the transport of the particle moving in the system, we present the phase-space maps of trajectories for different r in Fig. 3. The initial position $x(0)$ and initial velocity $v(0)$ of all

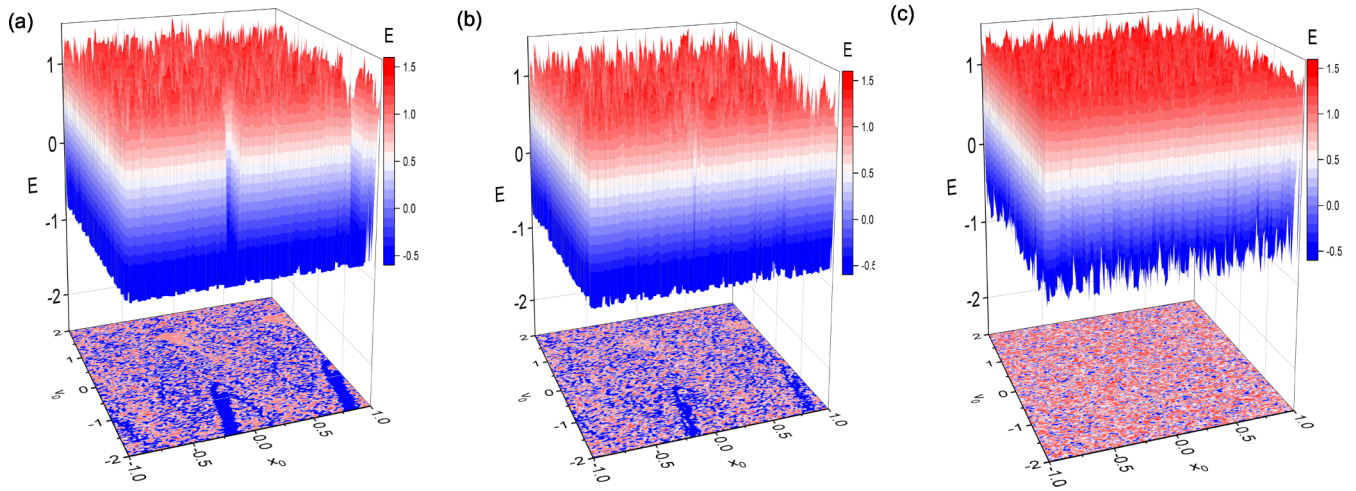

FIG. 2. The rugged energy landscape depending on the initial position and velocity for different roughnesses $\varepsilon = 0.0$ (a), 0.003 (b), and 0.010 (c). The parameters are identical to those in Figs. 2(d)–2(f).

trajectories are both 0.0. For different r, Figs. 3(a)–3(d) and 3(e)–3(h) show the phase-space map without and with the roughness from $t = 0$ to 100, respectively. Figure 3(a) shows that the particle moves between $x(t) = -1$ and 8. For $r = 0.05$, Fig. 3(b) displays that it moves between $x(t) = -4$ and 7. Notice that the horizontal line in phase-space map denotes the stochastic resetting, such as the mark in red arrow. With $r = 0.1$, Fig. 3(c) shows that it moves between $x(t) = -1$ and 22, meaning that the particle moves farther than that for $r = 0.05$. It should be noted that as r increases, there may be a kinetic phase transition from negative to positive mobility. However, Fig. 3(d) shows that the distance for $r = 0.2$ is smaller than that for $r = 0.1$. Therefore, these results reveal that the stochastic resetting can affect kinetics behaviors.

Let us turn to the system with roughness. For $\varepsilon = 0.2$, Fig. 3(e) shows that the particle stays in the initial well without stochastic resetting. However, the particle moves in the system with stochastic resetting. For example, at $r = 0.05$, the particle moves between $x = -5$ and 1. Notice that there are trivial fluctuations in the trajectory due to the existence of the rough potential. On the contrary, the trajectories are smooth in the system without the roughness [Figs. 3(a)–3(d)]. With $r = 0.10$, the particle moves between $x = 0.0$ and 5.0 [Fig. 3(g)]. As r further increases ($r = 0.20$), the particle moves between $x = -5$ to 5 [Fig. 3(h)]. These findings reveal that through stochastic resetting, the particle may be reset to a basin where the particle moves in the negative direction of the position, to a basin where the particle moves in the positive direction, or to a basin where it cannot move.

To better understand how the energy affects the transport of the particle, we present the phase-space map and the input power of stochastic resetting in Figs. 3(i)–3(p) from $t = 0$ to $t = 1000$. Without stochastic resetting ($r = 0.0$), Fig. 3(i) shows that for $F = 0.4$, the particle moves from $x \simeq 0.0$ to -350.0. This suggest that an anomalous mobility arises. At $r = 0.05$, Fig. 3(j) displays that the particle moves between $x = -120$ to 50. We also calculate the power of the stochastic resetting and obtain $P \approx 0.082$. For $r = 20$, Fig. 3(k) shows that the particle moves between $x = -130$ to 340. The corresponding power P is approximatively 0.559. On further increasing r (e.g., $r = 50$), the particle moves between $x = -110$ and 230. This means that its distance is smaller than that of $r = 20$. The corresponding power is nearly 0.16, which is also smaller than that of $r = 20$. In fact, the power may not be convergent for a finite sampling of the stochastic resetting (e.g., $t = 1000$).

With the roughness $\varepsilon = 0.2$, Fig. 3(m) shows that for $r = 0.0$, the particle stays in the initial well and no transport occurs. This is the case where the particle locates at the blue spike of the energy landscape in Fig. 2. However, for $r = 0.05$, Fig. 3(n) displays that the particle moves between $x = -20$ and 20 and the transport of the particle occurs. This means that there may be a kinetic phase transition from no transport to a finite net transport [67,68]. The corresponding power of the stochastic resetting is nearly 0.125. This finding reveals that the energy of the particle increases with the increase of the stochastic resetting. At $r = 20$, Fig. 3(o) shows that the particle moves between $x = -190$ and 210. And the power is approximately 0.664. However, as r further increases, the transport decreases. For example, with $r = 50$, Fig. 3(o) shows that the particle moves between $x = -160$ and 150. The corresponding power is nearly 0.426. We analyze these findings as follows.

These findings raise the natural question: What is the underlying mechanism behind the occurrence of these phenomena? Why the stochastic resetting leads to a kinetic phase transition and suppresses the motion of the particle? These results mentioned above show that through the stochastic resetting, the particle, located in a basin with a running state of a large velocity, may be reset to a basin with a running state of a small velocity. From an energy point of view, a particle, located at a low-energy regime of the energy landscape, is reset to a high-energy regime. Moreover, the particle moving from the left to the right is reset from the right to the left well or from the left to the right well. Overall, when the resettings from the right to left well are more than those from the left to the right well, the distance of the moving particle becomes smaller than that without this resetting with the identical time. Surely, there exists another possibility that the particle, lo-

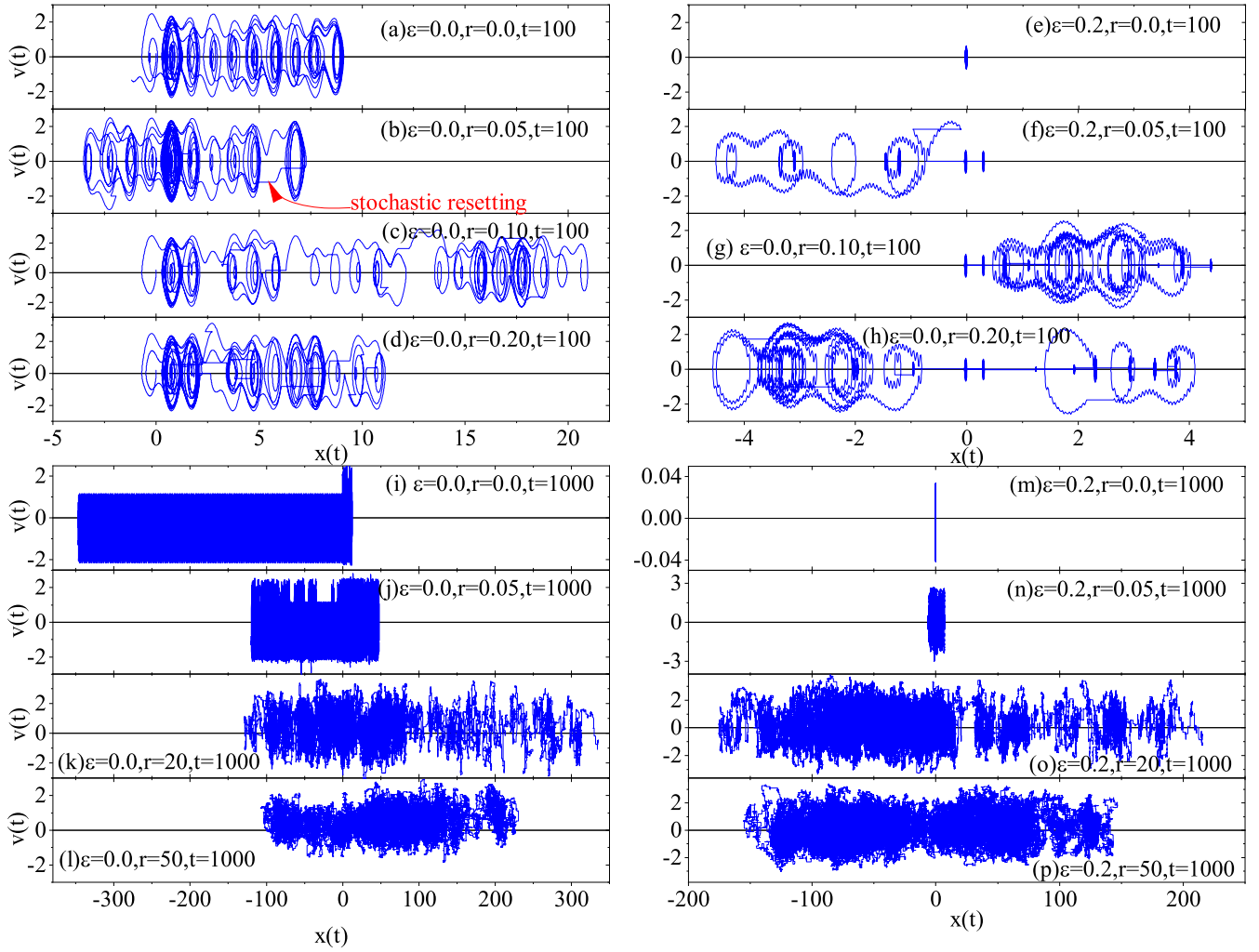

FIG. 3. The phase map with $\varepsilon = 0.0$ for different resetting probabilities $r = 0.0$ [(a) and (i)], 0.5 [(b) and (j)], 20 [(c) and (k)], and 50 [(d) and (l)] for $t = 100$ and 1000, respectively. The phase map with $\varepsilon = 0.2$ for different resetting probabilities $r = 0.0$ [(e) and (m)], 0.5 [(f) and (n)], 20 [(g) and (o)], and 50 [(h) and (p)] for $t = 100$ and 1000, respectively. Other parameters are $D = 0.0$ and $F = 0.4$.

cated at a basin with a running state of the small velocity, may be reset to a basin with the running state of the large velocity. Therefore, our results uncover that the choice of this initial state is the reason we obtain these results. Namely, due to the existence of the basins of attraction in the system, the unpredictability of the system results from the random initial states.

In brief, to answer the question of what is the underlying mechanism behind the occurrence of these phenomena, we present the phase-space map of trajectories to interpret these phenomena in Fig. 3. Based on the above analyses, we propose the predominant mechanism behind these phenomena. The significance of the mechanism is twofold. From a dynamical point of view, the particle, moving in the system with basins of attraction, is reset to a basin with a running state of a small or large velocity, which is different from the initial running state. From the energy point of view, the particle is reset to a new energy state (i.e., a high-energy state), which is different from the initial energy state (i.e., a low-energy state). Therefore, this resetting can lead to a new running state of the particle, meaning that it can result in a new state of motion which is different from the initial state of motion. Thus we employ this mechanism to explain the transports of the particle below.

To understand the transport of the particle moving in the system with the stochastic resetting and the roughness, Fig. 4 shows the two-dimensional (2D) maps of the average velocity. Figures 4(a)–4(c) show the velocity as a function of ε and F for different r. Without r, Fig. 4(a) shows that there exists a negative mobility for the system without or with trivial roughness ε, and no transport arises for $\varepsilon > 0.045$. Additionally, we also find that the roughness enhances the transport in certain regimes. For example, at $F = 0.5$, the flux is negative first (blue) and then becomes zero (green), furthermore positive (red), and finally zero (green) with the increase of the roughness. These findings reveal that the roughness ε weakens and eliminates negative mobility and also enhances and vanishes the transport in certain parameter regimes. At $r = 0.1$, Fig. 4(b) shows that negative mobility is almost eliminated and the roughness enhances the transport in certain parameter regimes. Interestingly, this resetting can induce the emergence of the transport in the system with large roughness (e.g., $\varepsilon > 0.045$), where no flux appears for $\varepsilon > 0.045$ in Fig. 4(a). The reason we obtain this finding is the underlying mechanism

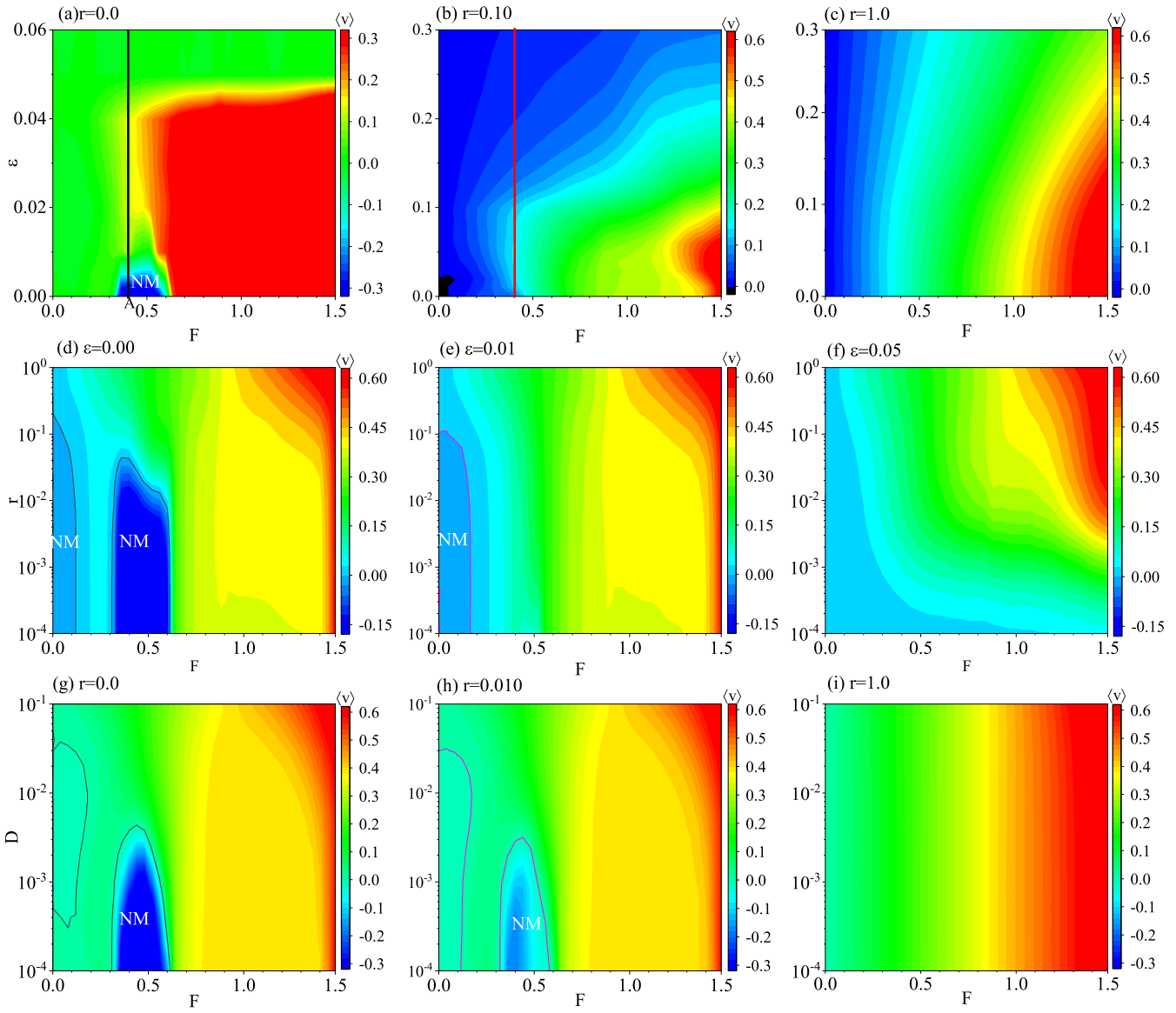

FIG. 4. Two-dimensional map of the average velocity $\langle v\rangle$ of the particle as a function of the bias F and the roughness ε corresponding to resetting probabilities $r = 0.0$ (a), 0.10 (b), and 1.0 (c). Two-dimensional map of $\langle v\rangle$ as a function of the bias F and resetting probabilities r with different roughnesses $\varepsilon = 0.0$ (d), 0.01 (e), and 0.05 (f). Two-dimensional map of $\langle v\rangle$ as a function of the bias F and the noise intensity D with different resetting probabilities $r = 0.0$ (g), 0.01 (h), and 1.0 (i).

we proposed in Fig. 2 and 3, which the stochastic resetting may be the process of the particle reset from a running state $v \simeq 0$ to one with $v \neq 0$. Namely, it drives the system into an out-of-equilibrium state which leads to the occurrence of the flux. For $r = 1.0$, Fig. 4(c) shows the flux still appears at $\varepsilon = 0.3$ where no flux arises in Fig. 4(b) for $r = 0.1$. In brief, the findings reveal that the roughness and stochastic resetting can weaken or eliminate negative mobility and enhance or vanish the transport. Moreover, the roughness also weakens and eliminates transport. The mechanism of Fig. 3 can explain why the system with the stochastic resetting appears transport where no transport arises in the system without this resetting. More insight into these findings is presented in Figs. 4(d)–4(f).

We present a 2D map of the velocity as a function of r and F for different roughnesses ε in Figs. 4(d)–4(f). Without the roughness ($\varepsilon = 0.0$), Fig. 4(d) shows that negative mobility appears in trivial stochastic resetting and disappears in large stochastic resettings. For $\varepsilon = 0.01$, Fig. 4(e) displays that negative mobility is weakened. As the roughness increases, negative mobility disappears, as shown in Fig. 4(f). In a word, the stochastic resetting could weaken or eliminate negative mobility. It also enhances the transport of the particle.

To settle the question of how the noise affects the transport of the particle moving in the system, we present a 2D map of the velocity as a function of D and F in Figs. 4(g)–4(i). Without the stochastic resetting ($r = 0.0$), Fig. 4(g) shows that the negative mobility appears for a weak noise and disappears for a strong noise. With $r = 0.01$, Fig. 4(h) displays that the negative mobility is weakened for a weak noise and rapidly disappears with the increase the the noise. For $r = 1$, Fig. 4(i)

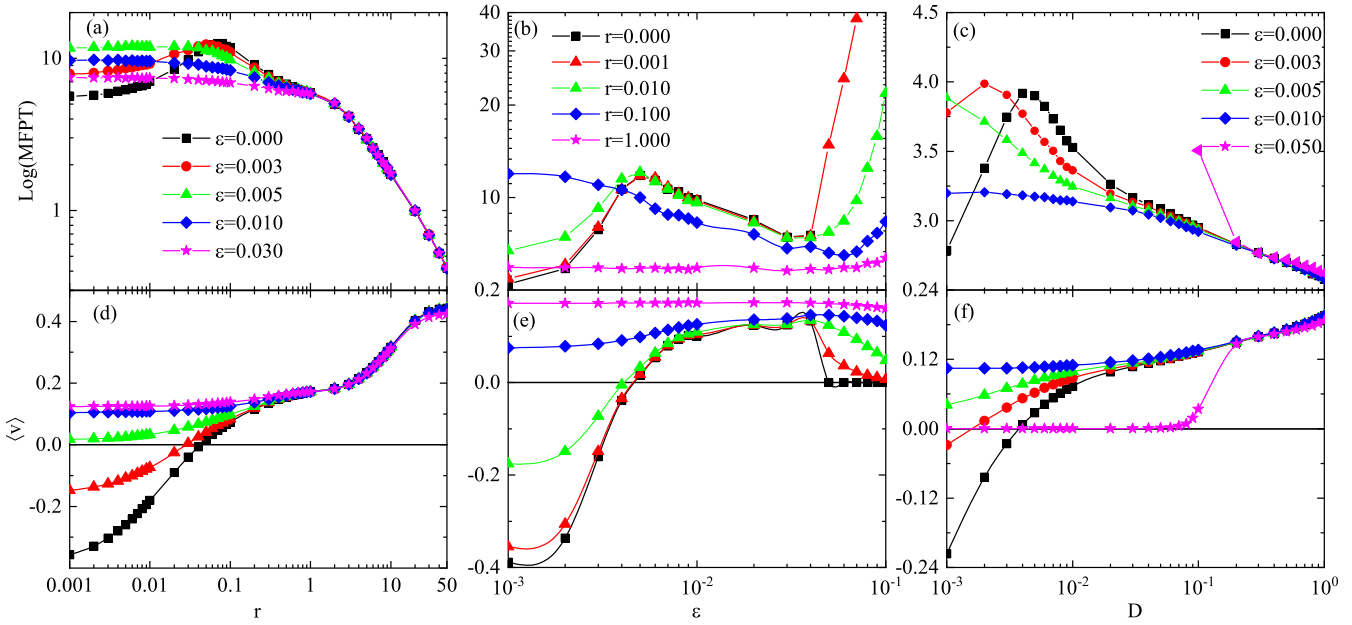

FIG. 5. The average velocity $\langle v\rangle$ and MFPT of the particle as functions of the stochastic resetting probability r with different roughnesses ε [(a) and (d)] for $D = 0.0001$. The average velocity $\langle v\rangle$ and MFPT of the particle as functions of the roughness ε with different resetting probabilities r [(b) and (e)] for $D = 0.0001$. The average velocity $\langle v\rangle$ and MFPT of the particle as functions of the noise intensity D with different roughness ε [(c) and (f)] for $r = 0.0$, respectively. The other parameter is $F = 0.4$. Log(MFPT) denotes the natural logarithm of MFPT.

shows that the negative mobility totally disappears. In a word, the noise can weaken or vanish negative mobility. It also enhances the transport of the particle in certain parameter regimes.

Next, we investigate the MFPT and kinetic phase transition in Fig. 5. We calculate the MFPT using the method in the earlier work [69], where the exit time of the particle is the escape time through either one of the box boundaries. The exit time is equivalent to the first passage time. Based on the initial and final positions of the work [41], MFPT is the ensemble average time from the starting point $x_0 = \arccos(F/2\pi)/(2\pi)$ with $v_0 = 0.0$ to the left or to the right boundary located at $x_{L,R} = x_0 \mp L$, where L is the period of the substrate potential. Figure 5(a) shows the MFPT as a function of r for different ε. Without the roughness ($\varepsilon = 0.0$), the MFPT increases first and then decreases with the increase of r. This implies that there exists a maximum. Namely, the stochastic resetting leads to the enhanced stability of the system. However, with the roughness (i.e., $\varepsilon = 0.005$), the MPFT is a constant first and then decreases with the increase of r. On further increasing ε, the MFPT almost decreases with increasing r (i.e., $\varepsilon = 0.030$). Namely, the roughness weakens and eliminates the stability of the system. Figure 5(b) displays the MPFT as functions of the roughness ε for different r. Without or with a small resetting rate (i.e., $r = 0.001$ or 0.010), the MFPT increases first, then decreases, and finally increases with the increase of the roughness ε. That is, there exists a maximum and a minimum for varying ε. The finding reveals that the roughness leads to the enhanced stability of the system and the resonant-like activation. At $r = 0.100$, the MFPT decreases first and then increases. This means that the roughness-enhanced stability of the system vanishes and the resonant-like activation still occurs. As the probability r increases (e.g., $r = 1.0$), both phenomena do not arise. Figure 5(c) shows the MFPT as a function of the noise intensity for different roughnesses. Without ε, MFPT shows that there exists a maximum for varying D. Namely, the noise leads to the enhanced stability of the system. As the roughness increases, this phenomenon vanishes.

To gain more insight into the kinetics corresponding to these findings, we present their fluxes in Figs. 5(d)–5(f). Without ε, Fig. 5(d) shows there exists a current reversal with varying probability r. From the view of kinetics, a kinetic phase transition from negative flux to positive flux occurs, and this is continuous (second order). As the roughness increases, the negative mobility disappears, and the flux increases with the increase of r. We also find that all curves almost overlap in the regime r ranging from 0.03 to 10. This suggests that the stochastic resetting is dominant in this regime for the motion of the particle. By comparison, then combination of ε and r is dominant in other regimes. Figure 5(e) shows the flux as a function of ε for different r. Without r or trivial resetting probability (i.e., $r = 0.001$ or $r = 0.010$), there exist negative mobilities in trivial roughness and current reversals for the varying roughness. As r increases (i.e., $r = 1.0$), the flux monotonically decays with the increase of ε. In brief, the roughness leads to a kinetic phase transition from negative to positive mobility. This is, it weakens and eliminates negative mobility. These findings are excellently in agreement with the enhanced stability of the system and resonant-like activation of the MFPT in Fig. 5(b). Figure 5(f) shows the flux as a function of the noise intensity for different roughness ε. Without r, there exists a current reversal for varying D. Namely, a kinetic phase transition from negative flux to positive flux arises. As the roughness increases, the negative mobility disappears and the flux increases monotonically with increasing D (i.e.,

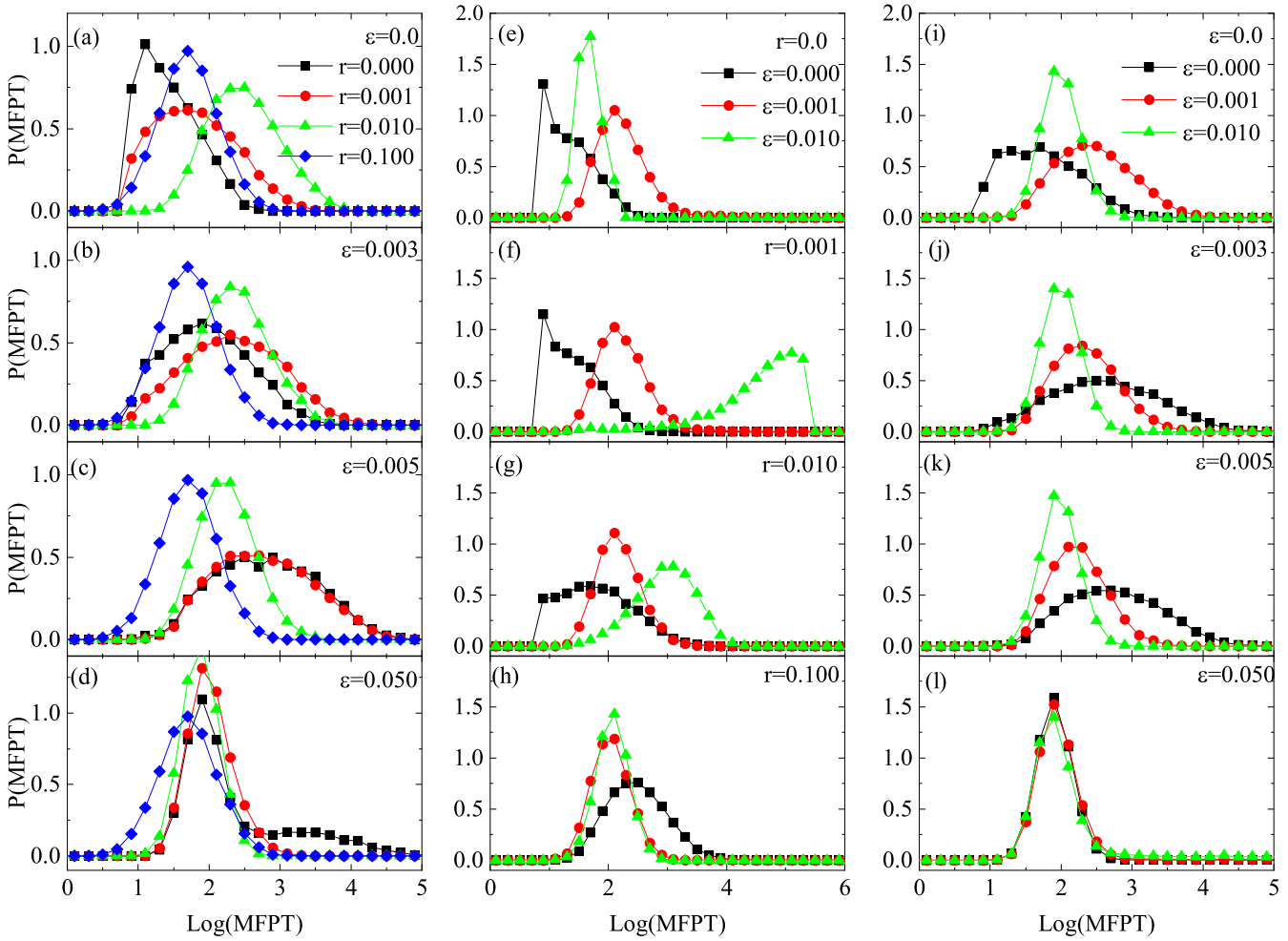

FIG. 6. The probability distributions of MFPTs, most of which corresponds to parameter setups in Fig. 5. The other parameters are same as those in Fig. 5. Log(MFPT) denotes the natural logarithm of MFPT.

$\varepsilon = 0.005$). On further increasing ε (i.e., $\varepsilon = 0.05$), there is no flux first and a finite net flux arises with the increase of D. Namely, there exists a kinetic phase transition from no flux to a finite net flux. All in all, the stochastic resetting, the roughness, and the noise can lead to a kinetic phase transition from negative to positive mobility or from no transport to a finite net transport. These transitions suggest that the stochastic resetting, the roughness, and the noise should tune enhanced stability of the system and resonant-like activation.

The Kramers escape theory, frequently characterized by MFPT, is of great importance in several research fields. To provide a full description of the MFPT, we present its probability distributions in Fig. 6, which correspond to certain points in Fig. 5. Figure 6(a) shows that as the probability r increases, the peaks of the distributions shift from the small MFPT to the large one and then from the large MFPT to the small one. Moreover, the height of the peaks transits from the high to the low first and then from the low to the high with an increase of r. This finding leads to the enhanced stability of the system and well agrees with that for $\varepsilon = 0.0$ in Fig. 5(a). For a small r, despite the results of Fig. 6(b) are basically identical to those of Fig. 6(a), the shift and the height of the distributions are smaller than those in Fig. 6(a). By comparison, they are identical to each other for the large r. These results are consistent with those for $\varepsilon = 0.003$ in Fig. 5(a). Figures 6(c) and 6(d) show that as r increases, the peaks shift from the large MFPT to the small one only. These findings imply that the MFPT monotonously decreases with the increase of r.

Figures 6(e)–6(h) correspond to several points in Fig. 5(b). As the roughness ε increases, Fig. 6(e) shows that the peaks of the distributions shift from the small MFPT to the large one first, then from the large MFPT to small one. However, for $r = 0.010$ and 0.100, Figs. 6(f) and 6(g) show that the peaks of the distributions transit from a small MFPT to a large one. Moreover, Fig. 6(h) shows that for $r = 0.100$, the peaks of the distributions shift from the large MFPT to the small one only. These results are in agreement with those in Fig. 5.

Figures 6(i)–6(l) correspond to certain points in Fig. 5(c). For $\varepsilon = 0.0$, Fig. 6(i) shows the peaks of the distributions shift from the small MFPT to the large one first and then from the large MFPT to the small one. As ε increases, Figs. 6(j) and 6(k) show that the peaks of the distributions transit from the large MFPT to the one only. For $\varepsilon = 0.050$, the peaks and the heights of the distributions trivially change.

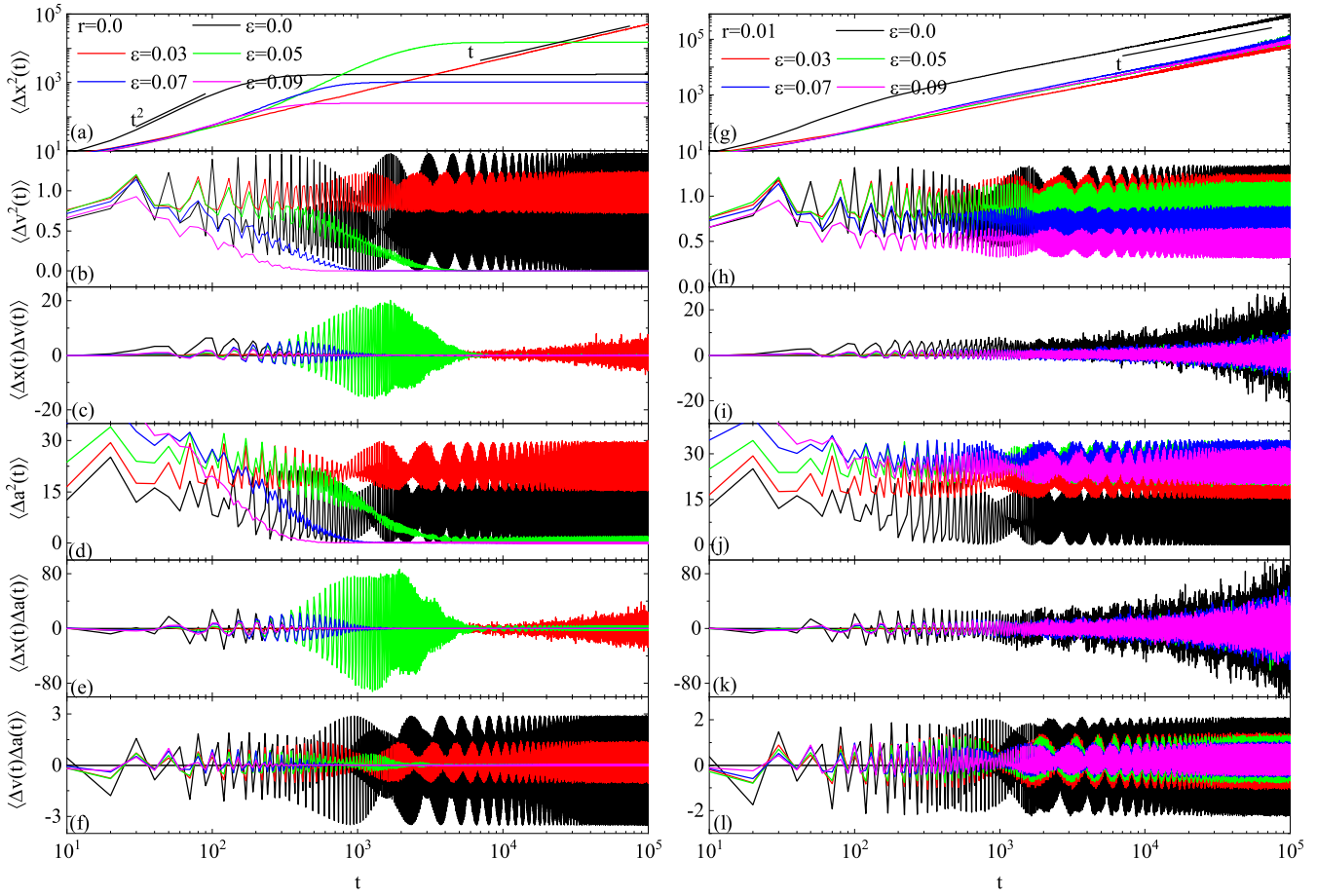

FIG. 7. The MSD [(a) and (g)], the mean-squared velocity [(b) and (h)], the variance of the position-velocity [(c) and (i)], the mean-squared acceleration [(d) and (j)], the variance of the position-acceleration [(e) and (k)], and the variance of the velocity-acceleration [(f) and (l)] without and with stochastic resetting. Other parameter are $D = 10^{-4}$ and $F = 0.4$.

These findings are consistent with those in Fig. 5(c). In brief, the probability distributions of MFPT also demonstrate that the stochastic resetting, roughness, and noise can tune the enhanced stability of the system and the resonance-like activation.

We now turn to several variances characterizing diffusions of the particle. It is well known that in previous works, most diffusions are characterized via the MSD. Actually, the variances, the skewness, and the kurtosis of the position, velocity, and acceleration are related to each other, and thus of particular interest are these physical quantities to understand the dynamical behaviors. We present several variances in Fig. 7 with and without r for different ε. Figure 7(a) shows that, without the roughness ($\varepsilon = 0.0$), the MSD scales as t^2 at intermediate time (e.g., t ranging from 30 to 90) and then becomes a constant at long time limit. We note that the flux arises for this parameter setup in Fig. 4. Therefore, this implies that the particle moves in a quasilinear or linear response regime, in which the motion of the particle is dominated by the bias, and the effect of the periodic potential is trivial. For $\varepsilon = 0.03$, the MSD scales as time, meaning that the diffusion is normal at long times. Moreover, for a large ε (e.g., $\varepsilon = 0.07$), the MSD scales as t^α ($1.0 < \alpha < 2.0$) at intermediate time and then becomes a constant at long time. The result indicates that the diffusion is superdiffusive at intermediate time and subdiffusive at long time and finally converges to zero. Of special interest is that one wonder whether the other variances (i.e., mean-squared velocity, etc.) can also qualitatively characterize these behaviors (e.g., subdiffusion, superdiffusion, ballistic diffusion, etc.). Therefore, we now turn to other variances. Figure 7(b) shows that $\langle \Delta v^2(t) \rangle$ persistently oscillates with an nontrivial amplitude for $\varepsilon = 0.00$, suggesting that the this oscillation corresponds to the point A in Fig. 4(a) that shows a negative mobility. $\langle \Delta v^2(t) \rangle$ for $\varepsilon = 0.03$ remain persistent oscillation with a trivial amplitude, suggesting that this oscillation corresponds to the normal diffusion. As ε further increases (i.e., $\varepsilon = 0.07$), $\langle \Delta v^2(t) \rangle$ oscillates in intermediate time and then decays to zero, which correspond to superdiffusion, subdiffusion, and no diffusion, respectively. Let us see $\langle \Delta x(t) \Delta v(t) \rangle$ with time for different ε in Fig. 7(c). For $\varepsilon = 0.00$, $\langle \Delta x(t) \Delta v(t) \rangle$ is zero. For $\varepsilon = 0.03$, the amplitudes for the oscillation of $\langle \Delta x(t) \Delta v(t) \rangle$ increase with time, suggesting that this behavior corresponds to the normal diffusion in Fig. 7(a). For a large ε (e.g., $\varepsilon = 0.05$), the oscillating amplitude of $\langle \Delta x(t) \Delta v(t) \rangle$ increases first, then decreases, and converges to zero, which correspond to superdiffusion, subdiffusion, and no diffusion, respectively. The behaviors of $\langle \Delta a^2(t) \rangle$ in Fig. 7(d) are almost identical

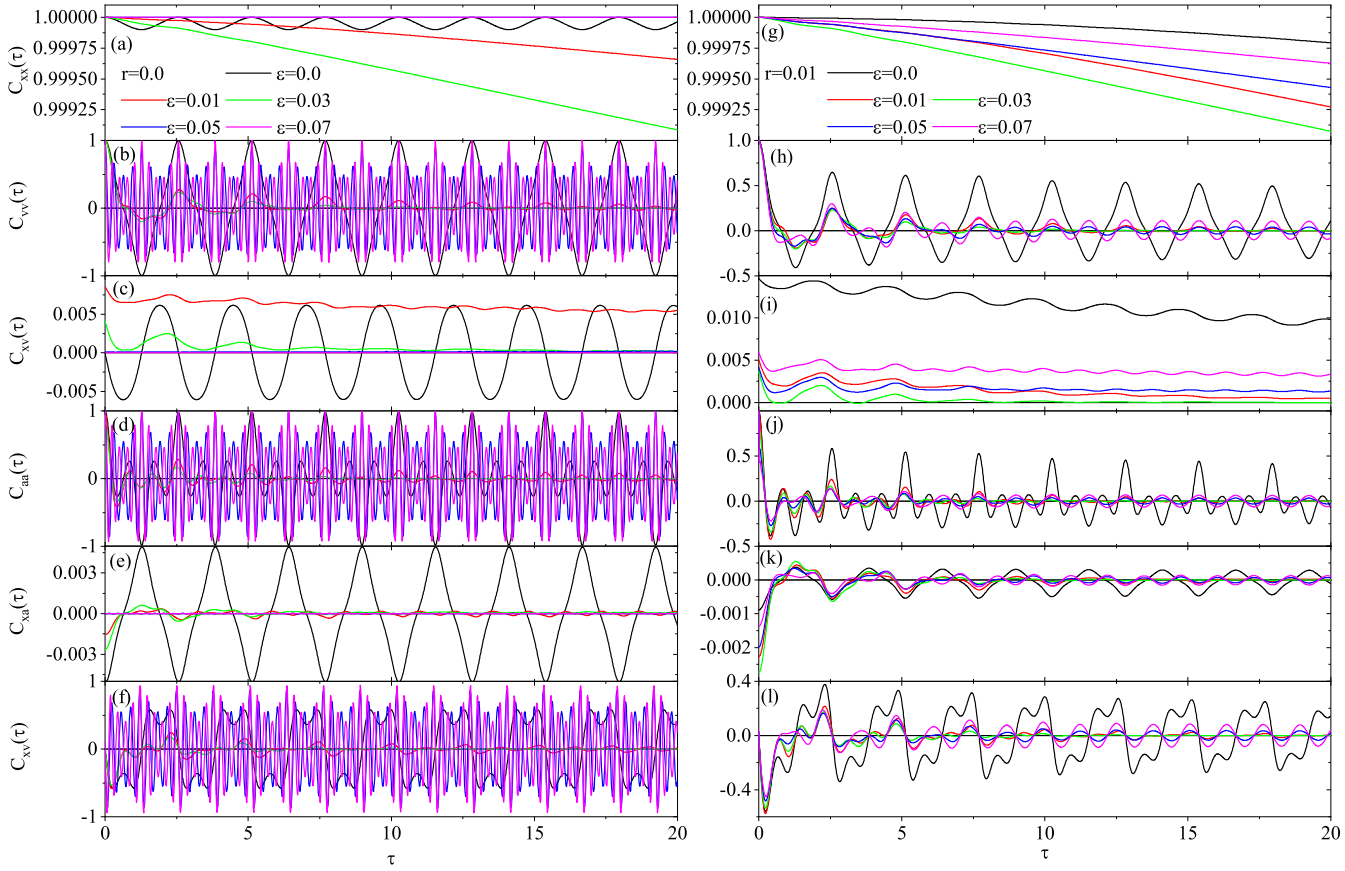

FIG. 8. The position autocorrelation function [(a) and (g)], the velocity autocorrelation function [(b) and (h)], the correlation function of the position-velocity [(c) and (i)], the acceleration autocorrelation function [(d) and (j)], the correlation functions of the position-acceleration [(e) and (k)], and velocity-acceleration [(f) and (l)] without and with stochastic resetting. Other parameter are $D = 10^{-4}$ and $F = 0.4$.

to those in Fig. 7(b), except their amplitudes are different. Moreover, the behaviors of $\langle \Delta x(t)\Delta a(t)\rangle$ in Fig. 7(e) are almost same as those of $\langle \Delta x(t)\Delta v(t)\rangle$ in Fig. 7(c), except their amplitudes are different. Figure 7(f) shows that for $\varepsilon = 0.00$, $\langle \Delta v(t)\Delta a(t)\rangle$ nontrivially oscillates with zero crossings. For $\varepsilon = 0.03$, $\langle \Delta v(t)\Delta a(t)\rangle$ trivially oscillates with zero crossings, and the oscillation tends to the positive direction, implying that positive mobility arises. Finally, with a large ε ($\varepsilon = 0.05$), $\langle \Delta v(t)\Delta a(t)\rangle$ trivially oscillates first and then decays to zero, corresponding to superdiffusion and no diffusion, respectively. In summary, when $\langle \Delta v^2(t)\rangle$ or $\langle \Delta a^2(t)\rangle$ converges to zero, the corresponding diffusions also converge to zero. By contrast, when they remain nontrivially persistent oscillations, the corresponding diffusions are normal. Additionally, when $\langle \Delta x(t)\Delta v(t)\rangle$, $\langle \Delta x(t)\Delta a(t)\rangle$, and $\langle \Delta v(t)\Delta a(t)\rangle$ coverage to zero, the corresponding diffusions are zero. When the amplitudes of their oscillations decrease, linearly increase, or exponentially increase with time, the corresponding diffusions are subdiffusive, normal, or superdiffusive, respectively. In brief, besides the MSD, mean-squared velocity, mean-squared acceleration, and the variance of the position-velocity, the position-acceleration, and the velocity-acceleration can also characterize the types of diffusions.

We now turn to the variances with a stochastic resetting. Figures 7(g)–7(l) show several variances with $r = 0.01$ for different ε. We present MSDs for different ε in Fig. 7(g). All curves basically scale as t at long time, which are different from those without stochastic resetting, most of which converge to a constant at long time limit. This finding suggests that a particle can move in the system with stochastic resetting, whereas it remains a well of the system without this condition. Thus the corresponding $\langle \Delta v^2(t)\rangle$ in Fig. 7(h), $\langle \Delta a^2(t)\rangle$ in Fig. 7(j), and $\langle \Delta v(t)\Delta a(t)\rangle$ in Fig. 7(l) persistently oscillate with time. Moreover, the amplitude of the oscillation for corresponding $\langle \Delta x(t)\Delta v(t)\rangle$ in Fig. 7(i) and $\langle \Delta x(t)\Delta a(t)\rangle$ in Fig. 7(k) linearly increase with time at long times. These findings suggest that the diffusion is normal.

To better understand how the roughness and the stochastic resetting affect the dynamics of the system, we now turn to the position autocorrelation function, velocity autocorrelation function, acceleration autocorrelation function, position-velocity correlation function, position-acceleration correlation function, and velocity-acceleration correlation function in Fig. 8. These correlation functions correspond to several points in Fig. 4 [the black line in Fig. 4(a) and the red line in Fig. 4(b)] and part of which correspond to anomalous transport. Without the stochastic resetting, Fig. 8(a) exhibits that for $\varepsilon = 0.0$, the correlation function trivially oscillates nearly 1.0, which corresponds to the negative mobility in Fig. 4(a). By contrast, for $\varepsilon = 0.01$ and 0.03, the correlation

functions decrease with time, corresponding to finite net transports in Fig. 4(a). The correlation function corresponding to a large ε (i.e., $\varepsilon = 0.05$) equals 1.0, corresponding to no flux in Fig. 4(a). In fact, this finding results from that the particle remains in a well of the system with time evolution. We now also present other correlation functions. Figure 8(b) shows the velocity autocorrelation function for different ε. The velocity autocorrelation functions corresponding to $\varepsilon = 0.01$ and 0.03 exhibit nonmonotonic decay with zero crossings, while they for $\varepsilon = 0.05$ and 0.07 oscillate and their amplitudes do not decay. Thus these findings suggest that the velocity autocorrelation function, which oscillates and does not decay, corresponds to no transport. However, there being an nonmonotonic decay with zero crossings, it corresponds to the occurrence of the flux. $C_{xv}(\tau)$ in Fig. 8(c), $C_{aa}(\tau)$ in Fig. 8(d), $C_{xa}(\tau)$ in Fig. 8(e), and $C_{va}(\tau)$ in Fig. 8(f) also demonstrate two key results. One is that these correlation functions exhibit an nonmonotonic decay, which corresponds to an finite net transport. The other is that they do not decay, which corresponds to no flux. The underlying reason we obtain these results is the following. For a particle jumping from a well to another well in the system, the corresponding correlation between two different moments is smaller than 1. On the contrary, for a particle remaining in a well of the system, this correlation equals 1 due to the autocorrelation of the identical quantities.

In the presence of stochastic resetting $r = 0.01$, these correlation functions are presented in Figs. 8(g)–8(l). Figure 8(g) displays that correlation functions with stochastic resetting decay faster than those without stochastic resetting in Fig. 8(a) with time. The reason is that the positions after stochastic resetting are not directly related to those before stochastic resetting. We also note that for a large ε (e.g., $\varepsilon = 0.07$), $C_{xx}(\tau)$ in Fig. 8(g) and $C_{vv}(\tau)$ in Fig. 8(h) with the stochastic resetting are different from those in Fig. 8(a) and Fig. 8(b) without the stochastic resetting, respectively. These results suggest that without the stochastic resetting, the particle maybe remain in the initial well and no flux thus arises. On the contrary, with the resetting, the particle can move from a well to another well and the flux consequently occurs. These findings agree with those in Fig. 4(b) (the red line). Furthermore, we find that other correlation functions with the stochastic resetting in Figs. 8(h)–8(l) decay faster than those without it in Figs. 8(b)–8(f), respectively. This results imply that the diffusion of the former is larger than that of the latter.

IV. CONCLUSION

We numerically investigate the anomalous transport of a particle in a system with a rough potential and the stochastic resetting by a random amplitude. The system with nonequilibrium fluctuation is driven by an external time-periodic force and an external bias. We analyze the transport of the particle via the chaotic dynamics, the basin of attraction, rugged energy landscape, phase-space map, average velocity, mean first passage time, various variances, and correlation functions.

The chaotic dynamics, basin of attraction, rugged energy landscape, and phase-space map show how the stochastic resetting leads to kinetic phase transitions, which is continuous. From the perspective of dynamics, through the stochastic resetting, a particle, located in a basin of attraction with a running state of the initial velocity (e.g., a small velocity), may be reset to a basin of attraction with a running state of the new velocity (i.e., a large velocity), which may be different the initial state. From the perspective of the energy landscape, the particle, located at an initial energy state (i.e., the low-energy state), may be reset to a new energy state (i.e., the high-energy state). The phase-space map shows how the particle is reset to a new state. These behaviors can lead to the resonant-like activation, the enhanced stability of the system, and kinetic phase transitions from no transport to a finite net transport or from negative mobility to positive mobility. Compared with the early works about the energy landscape with stochastic resetting [33], our results are twofold. First, it narrows the gap between a stochastic resetting leading to transports and the underlying physical mechanism. Second, it provides more insight into the process of the stochastic resetting and the transports.

We also discuss how the roughness and noise affect the transport. Our results reveal that the roughness can weaken, eliminate, and lead to the flux of the particle. These findings result from the chaotic properties and basin of attraction, implying that the dynamics is very sensitive to the trivial variations of the initial states and system parameters. The above mention results are interpreted through the basin of the attraction or rugged energy landscape. Finally, our results also reveal that noise can tune negative mobility and the flux.

Here we analyze our results via several variances (e.g., mean-squared velocity, the variance of the position-velocity, etc.) and find that all of them can qualitatively characterize the types of diffusion. There exist four behaviors in the variances of the position-velocity and the position-acceleration, which correspond to four types of diffusion. First, the case that the amplitude of their oscillation linearly increases with time denotes normal diffusion. Second, the case that they decrease with time indicates a subdiffusion. Third, the case that they exponentially increase is superdiffusion. The last that there exists no oscillation corresponds to zero diffusion. Moreover, the mean-squared velocity or acceleration oscillating with time corresponds to a finite net transport, whereas it with no oscillation with time is no diffusion. Furthermore, we also analyze our findings through several correlation functions, i.e., velocity autocorrelation function, the position-velocity correlation function, and so on. Due to the presence of periodic potential, the correlation functions exhibit nonmonotonic decay with zero crossings or no zero crossing. These findings reveal that stochastic resetting can give rise to the occurrence of the flux. The larger the power-law exponent of diffusion, the faster the oscillation of correlation functions. Therefore, these variances and correlation functions also characterize the transports and diffusions of the particle.

In conclusion, we numerically investigate anomalous mobilities and diffusions of the particle moving in a system with a rough potential and stochastic resetting. We focus on how the roughness, stochastic resetting, and noise affect mobility and diffusion and propose an underlying mechanism behind these transport and diffusion. The physical mechanism of our work can be generalized to a wide range of systems, such as

financial crashes owing to a fall in stock prices [70], a sudden reduction in population size owing to catastrophes [71], and a stochastic biological system modeling the excursions by uncorrelated random jumps [8]. It can also be extended to apply in social system. For example, the job hopping is important in computer clusters because it facilitates the reallocation of talent and resources toward firms with superior innovations [72]. This job hopping should be viewed as a stochastic resetting. Thus, a deep understanding of our work will actually be important to analyze the evolution in social system.

ACKNOWLEDGMENTS

This work was supported by the National Natural Science Foundation of China (Grant No. 12265017), Yunnan Fundamental Research Projects (Grant No. 2019FI002, No. 202101AS070018, and No. 202101AV070015), Xingdian Talents Support Program, and Yunnan Province Ten Thousand Talents Plan Young & Elite Talents Project and Yunnan Province Computational Physics and Applied Science and Technology Innovation Team.

[1] S. Reuveni, M. Urbakh, and J. Klafter, Role of substrate unbinding in Michaelis-Menten enzymatic reactions, Proc. Natl. Acad. Sci. USA **111**, 4391 (2014).

[2] T. Robin, S. Reuveni, and M. Urbakh, Single-molecule theory of enzymatic inhibition, Nat. Commun. **9**, 779 (2018).

[3] L. Kusmierz, S. N. Majumdar, S. Sabhapandit, and G. Schehr, First Order Transition for the Optimal Search Time of Lévy Flights with Resetting, Phys. Rev. Lett. **113**, 220602 (2014).

[4] B. De Bruyne, J. Randon-Furling, and S. Redner, Optimization in First-Passage Resetting, Phys. Rev. Lett. **125**, 050602 (2020).

[5] M. R. Evans and S. N. Majumdar, Diffusion with Stochastic Resetting, Phys. Rev. Lett. **106**, 160601 (2011).

[6] S. Gupta, S. N. Majumdar, and G. Schehr, Fluctuating Interfaces Subject to Stochastic Resetting, Phys. Rev. Lett. **112**, 220601 (2014).

[7] D. Gupta, C. A. Plata, and A. Pal, Work Fluctuations and Jarzynski Equality in Stochastic Resetting, Phys. Rev. Lett. **124**, 110608 (2020).

[8] M. Coppey, O. Bénichou, R. Voituriez, and M. Moreau, Kinetics of target site localization of a protein on DNA: A stochastic approach, Biophys. J. **87**, 1640 (2004).

[9] A. Lisica, C. Engel, M. Jahnel, É. Roldán, E. A. Galburt, P. Cramer, and S. W. Grill, Kinetics of Mechanisms of backtrack recovery by RNA polymerases I and II, Proc. Natl. Acad. Sci. USA **113**, 2946 (2016).

[10] É. Roldán, A. Lisica, D. Sánchez-Taltavull, and S. W. Grill, Stochastic resetting in backtrack recovery by RNA polymerases, Phys. Rev. E **93**, 062411 (2016).

[11] W. Wang, A. G. Cherstvy, H. Kantz, R. Metzler, and I. M. Sokolov, Time averaging and emerging nonergodicity upon resetting of fractional Brownian motion and heterogeneous diffusion processes, Phys. Rev. E **104**, 024105 (2021).

[12] D. Vinod, A. G. Cherstvy, W. Wang, R. Metzler, and I. M. Sokolov, Nonergodicity of reset geometric Brownian motion, Phys. Rev. E **105**, L012106 (2022).

[13] W. Wang, A. G. Cherstvy, R. Metzler, and I. M. Sokolov, Restoring ergodicity of stochastically reset anomalous-diffusion processes, Phys. Rev. Res. **4**, 013161 (2022).

[14] M. Magoni, S. N. Majumdar, and G. Schehr, Ising model with stochastic resetting, Phys. Rev. Res. **2**, 033182 (2020).

[15] L. Machura, M. Kostur, P. Talkner, J. Łuczka, and P. Hänggi, Absolute Negative Mobility Induced by Thermal Equilibrium Fluctuations, Phys. Rev. Lett. **98**, 040601 (2007).

[16] J. Spiechowicz, P. Hänggi, and J. Łuczka, Coexistence of absolute negative mobility and anomalous diffusion, New J. Phys. **21**, 083029 (2019).

[17] Y. Luo, C. Zeng, and B. Li, Negative rectification and anomalous diffusion in nonlinear substrate potentials: Dynamical relaxation and information entropy, Phys. Rev. E **105**, 024204 (2022).

[18] Y. Luo, C. Zeng, and B.-Q. Ai, Strong-chaos-caused negative mobility in a periodic substrate potential, Phys. Rev. E **102**, 042114 (2020).

[19] V. Domazetoski, A. Masó-Puigdellosas, T. Sandev, V. Méndez, A. Iomin, and L. Kocarev, Stochastic resetting on comblike structures, Phys. Rev. Res. **2**, 033027 (2020).

[20] A. A. Dubkov, N. V. Agudov, and B. Spagnolo, Noise-Enhanced Stability in Fluctuating Metastable States, Phys. Rev. E **69**, 061103 (2004).

[21] L. Magazzù, P. Hänggi, B. Spagnolo, and D. Valenti, Quantum resonant activation, Phys. Rev. E **95**, 042104 (2017).

[22] M. Dahlenburg, A. V. Chechkin, R. Schumer, and R. Metzler, Stochastic resetting by a random amplitude, Phys. Rev. E **103**, 052123 (2021).

[23] C. S. Holling, Resilience and stability of ecological systems, Annu. Rev. Ecol. Syst. **4**, 1 (1973).

[24] F. Lillo and R. N. Mantegna, Dynamics of a financial market index after a crash, Physica A **338**, 125 (2004).

[25] L. Lin, R. E. Ren, and D. Sornette, The volatility-confined LPPL model: A consistent model of 'explosive' financial bubbles with mean-reverting residuals, Int. Rev. Fin. Anal. **33**, 210 (2014).

[26] E. Kussell and S. Leibler, Phenotypic diversity, population growth, and information in fluctuating environments, Science **309**, 2075 (2005).

[27] M. Hu and J.-D. Bao, Diffusion crossing over a barrier in a random rough metastable potential, Phys. Rev. E **97**, 062143 (2018).

[28] I. Goychuk, V. O. Kharchenko, and R. Metzler, Persistent Sinai-type diffusion in Gaussian random potentials with decaying spatial correlations, Phys. Rev. E **96**, 052134 (2017).

[29] V. Zaburdaev, S. Denisov, and P. Hänggi, Space-time velocity correlation function for random walks, Phys. Rev. Lett. **110**, 170604 (2013).

[30] F. Kindermann, A. Dechant, M. Hohmann, T. Lausch, D. Mayer, F. Schmidt, E. Lutz, and A. Widera, Nonergodic diffusion of single atoms in a periodic potential, Nat. Phys. **13**, 137 (2017).

[31] Y. Gao, Y. Jiao, and Y. Liu, Ultraefficient reconstruction of effectively hyperuniform disordered biphase materials via non-Gaussian random fields, Phys. Rev. E **105**, 045305 (2022).

[32] C. P. Massen and J. P. K. Doye, Power-law distributions for the areas of the basins of attraction on a

potential energy landscape, Phys. Rev. E **75**, 037101 (2007).
[33] A. Pal, Diffusion in a potential landscape with stochastic resetting, Phys. Rev. E **91**, 012113 (2015).
[34] B. Derrida, Random-energy model: An exactly solvable model of disordered systems, Phys. Rev. B **24**, 2613 (1981).
[35] S. N. Gomes, S. Kalliadasis, G. A. Pavliotis, and P. Yatsyshin, Dynamics of the Desai-Zwanzig model in multiwell and random energy landscapes, Phys. Rev. E **99**, 032109 (2019).
[36] A. Szulc, O. Gat, and I. Regev, Forced deterministic dynamics on a random energy landscape: Implications for the physics of amorphous solids, Phys. Rev. E **101**, 052616 (2020).
[37] I. Goychuk and V. O. Kharchenko, Anomalous Features of Diffusion in Corrugated Potentials with Spatial Correlations: Faster than Normal, and Other Surprises, Phys. Rev. Lett. **113**, 100601 (2014).
[38] G. R. Archana and D. Barik, Roughness in the periodic potential enhances transport in a driven inertial ratchet, Phys. Rev. E **104**, 024103 (2021).
[39] Y. Li, Y. Xu, J. Kurths, and X. Yue, Lévy-noise-induced transport in a rough triple-well potential, Phys. Rev. E **94**, 042222 (2016).
[40] J. Liu, F Li, Y. Zhu, and B. Li, Enhanced transport of inertial Lévy flights in rough tilted periodic potential, J. Stat. Mech.: Theory Exp. (2019) 033211.
[41] Y. Li, Y. Xu, and J. Kurths, Roughness-enhanced transport in a tilted ratchet driven by Lévy noise, Phys. Rev. E **96**, 052121 (2017).
[42] S. Havlin and D. ben-Avraham, Diffusion in disordered media, Adv. Phys. **36**, 695-798 (1987).
[43] O. Bénichou and R. Voituriez, From first-passage times of random walks in confinement to geometry-controlled kinetics, Phys. Rep. **539**, 225 (2014).
[44] A. L. Lloyd and R. M. May, Epidemiology-how viruses spread among computers and people, Science **292**, 1316 (2001).
[45] M. F. Shlesinger, Search research, Nature (London) **443**, 281 (2006).
[46] P. S. Burada and B. Lindner, Escape rate of an active Brownian particle over a potential barrier, Phys. Rev. E **85**, 032102 (2012).
[47] S. Condamin, O. Bénichou, V. Tejedor, R. Voituriez and J. Klafter, First-passage times in complex scale-invariant media, Nature (London) **450**, 77 (2007).
[48] S. Reuveni, Optimal Stochastic Restart Renders Fluctuations in First Passage Times Universal, Phys. Rev. Lett. **116**, 170601 (2016).
[49] S. Ahmad, I. Nayak, A. Bansal, A. Nandi, and D. Das, First passage of a particle in a potential under stochastic resetting: A vanishing transition of optimal resetting rate, Phys. Rev. E **99**, 022130 (2019).
[50] A. Pal and V. V. Prasad, First passage under stochastic resetting in an interval, Phys. Rev. E **99**, 032123 (2019).
[51] A. S. Bodrova and I. M. Sokolov, Resetting processes with noninstantaneous return, Phys. Rev. E **101**, 052130 (2020).
[52] A. Masó-Puigdellosas, D. Campos, and V. Méndez, Transport properties and first-arrival statistics of random motion with stochastic reset times, Phys. Rev. E **99**, 012141 (2019).
[53] V. Méndez, A. Masó-Puigdellosas, T. Sandev, and D. Campos, Continuous time random walks under Markovian resetting, Phys. Rev. E **103**, 022103 (2021).
[54] Y. Han, A. M. Alsayed, M. Nobili, J. Zhang, T. C. Lubensky, and A. G. Yodh, Brownian motion of an ellipsoid, Science **314**, 626 (2006).
[55] R. Belousov, E. G. D. Cohen, C.-S. Wong, J. A. Goree, and Y. Feng, Skewness of steady-state current fluctuations in nonequilibrium systems, Phys. Rev. E **93**, 042125 (2016).
[56] M. Cristelli, A. Zaccaria, and L. Pietronero, Universal relation between skewness and kurtosis in complex dynamics, Phys. Rev. E **85**, 066108 (2012).
[57] T. Turiv, I. Lazo, A. Brodin, B. I. Lev, V. Reiffenrath, V. G. Nazarenko, and O. D. Lavrentovich, Effect of collective molecular reorientations on Brownian motion of colloids in nematic liquid crystal, Science **342**, 1351 (2013).
[58] Y. Luo, C. Zeng, and B. Li, A perfect probe: Resonance of underdamped scaled Brownian motion, Europhys. Lett. **137**, 21002 (2022).
[59] T. Franosch, M. Grimm, M. Belushkin, F. M. Mor, G. Foffi, L. Forró, and S. Jeney, Resonances arising from hydrodynamic memory in Brownian motion, Nature (London) **478**, 85 (2011).
[60] L. Canet, V. Rossetto, N. Wschebor, and G. Balarac, Spatiotemporal velocity-velocity correlation function in fully developed turbulence, Phys. Rev. E **95**, 023107 (2017).
[61] G. Afek, J. Coslovsky, A. Courvoisier, O. Livneh, and N. Davidson, Observing Power-Law Dynamics of Position-Velocity Correlation in Anomalous Diffusion, Phys. Rev. Lett. **119**, 060602 (2017).
[62] A. Lukin, M. Rispoli, R. Schittko, M. Eric Tai, A. M. Kaufman, S. Choi, V. Khemani, J. Léonard, and M. Greiner, Probing entanglement in a many-body-localized system, Science **364**, 256 (2019).
[63] Z. Ma, Y. Luo, C. Zeng, and B. Zheng, Spatiotemporal diffusion as early warning signal for critical transitions in spatial tumor-immune system with stochasticity, Phys. Rev. Res. **4**, 023039 (2022).
[64] A. Słapik, J. Łuczka, P. Hänggi, and J. Spiechowicz, Tunable mass separation via negative mobility, Phys. Rev. Lett. **122**, 070602 (2019).
[65] R. L. Honeycutt, Stochastic Runge-Kutta algorithms. ii. Colored noise, Phys. Rev. A **45**, 604 (1992).
[66] A. Fuliński, Fractional Brownian motions: Memory, diffusion velocity, and correlation functions, J. Phys. A: Math. Theor. **50**, 054002 (2017).
[67] T. Vicsek, A. Czirók, E. Ben-Jacob, I. Cohen, and O. Shochet, Novel Type of Phase Transition in a System of Self-Driven Particles, Phys. Rev. Lett. **75**, 1226 (1995).
[68] G. Grégoire and H. Chaté, Onset of Collective and Cohesive Motion, Phys. Rev. Lett. **92**, 025702 (2004).
[69] B. Dybiec, E. Gudowska-Nowak, and I. M. Sokolov, Transport in a Lévy ratchet: Group velocity and distribution spread, Phys. Rev. E **78**, 011117 (2008).
[70] D. Sornette, *Why Stock Markets Crash: Critical Events in Complex Financial Systems*, (Princeton University Press, Princeton, NJ, 2003).
[71] M. E. J. Newman and R. G. Palamer, *Modeling Extinction* (Oxford University Press, Oxford, UK, 2003).
[72] B. Fallick, C. A. Fleischman, and J. B. Rebitzer, Job-hopping in Silicon Valley: Some evidence concerning the microfoundations of a high-technology cluster, Rev. Econ. Stat. **88**, 472 (2006).